

Supporting Information

Simple Synthesis and Surface Facet-tuning of Ultrathin Alloy-shells of Au@AuPd Nanoparticles *via* Silver-assisted Co-Reduction onto Facet-controlled Au Nanoparticles

Cuixia Bi,^a Yahui Song,^a Hongpeng He,^a Chenshuo Wu,^a Wei Du,^b Lihui Huang,^c Helmuth Moehwald^d and Haibing Xia^{a,*}

^aState Key Laboratory of Crystal Materials, Shandong University, Jinan, 250100, P. R China;

^bSchool of Environment and Material Engineering, Yantai University, Yantai 264005, Shandong, China.

^cSchool of Environmental Science and Engineering, Shandong University, Jinan, 250100, P. R. China.

^dMax Planck Institute of Colloids and Interfaces, Potsdam-Golm Science Park, 14476 Potsdam, Germany.

Corresponding Author:* (H. X.) E-mail: hbxia@sdu.edu.cn

Fig. S1 TEM image (a) and extinction spectrum (b) of as-prepared Au NRs.

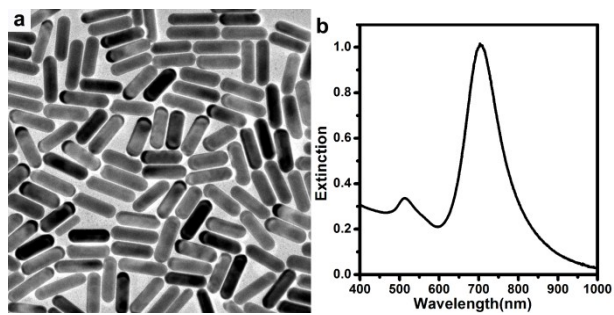
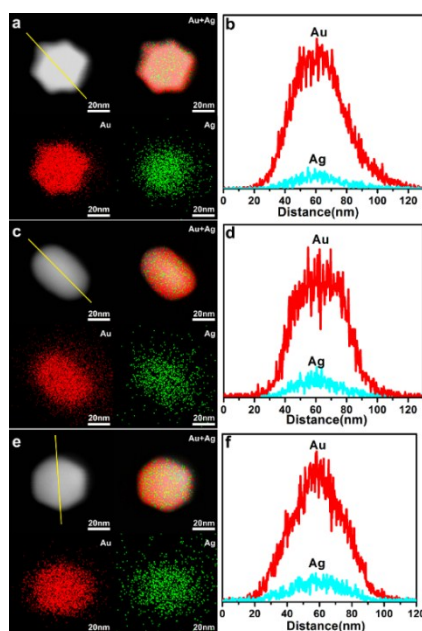
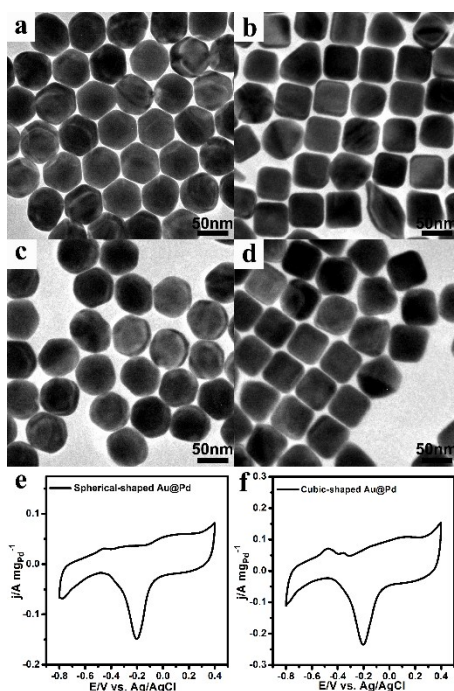


Fig. S2 HAADF-STEM-EDS mapping images (a, c and e) and HAADF-STEM images with cross-sectional compositional line profiles (b, d and f) of HOH-shaped Au NPs (a and b), ETHH-shaped Au NPs (c and d), and OCT-shaped Au NPs (e and f).



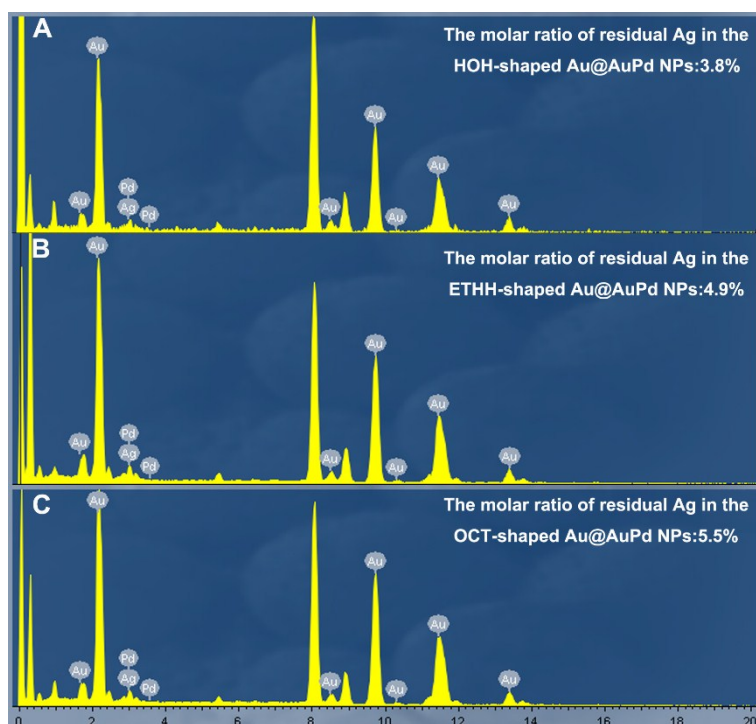
For synthesis of HOH-shaped, ETHH-shaped, and OCT-shaped Au NPs, Ag^+ ions were often used to control their morphology, thus Ag atoms should be present in the as-prepared Au NPs. The composition of the resulting HOH-shaped, ETHH-shaped, and OCT-shaped Au NPs was investigated by energy dispersive X-ray spectroscopy (EDS) and Inductively coupled plasma atomic emission spectroscopy (ICP-AES). Fig. S2 shows typical HAADF-STEM-EDS mapping images of HOH-shaped Au NPs (Fig. S2a and b), ETHH-shaped Au NPs (Fig. S2c and d), and OCT-shaped Au NPs (Fig. S2e and f), respectively. As expected, the element of Au and Ag can be observed, confirming the existence of these two elements. In addition, their cross-sectional compositional line profiles (Fig. S2b, d and f) revealing elemental Ag bears a distribution similar to elemental Au, thus confirming that elemental Ag is present on the surface of Au NPs. On the basis of the EDS results, the atomic fractions of Ag in the as-prepared HOH-, ETHH-, and OCT-shaped Au NPs are about 4.5%, 6.0%, and 8.4%, respectively. The results are the same as those obtained by ICP-AES.

Fig. S3 TEM images of spherical-shaped Au NPs (a), cubic-shaped Au NPs (b), spherical-shaped Au@Pd NPs (c), and cubic-shaped Au@Pd NPs (d). CV curves (e and f) of GCEs modified by spherical-shaped Au@Pd NPs and cubic-shaped Au@Pd NPs measured in 0.50 M N₂-saturated KOH aqueous solution at room temperature. The current densities (e and f) were normalized by the Pd mass loaded on GCE. The resulting spherical-shaped Au@Pd NPs and cubic-shaped Au@Pd NPs were obtained by co-reduction of Au(III) ions and Pd(II) ions onto the corresponding preformed Au cores.



Only Pd oxidation peaks are shown in the CV curves (Fig. S3e and f) of spherical-shaped Au@Pd NPs and cubic-shaped Au@Pd NPs measured in an alkaline medium, indicating the formation of core-shell Au@Pd structure, although Au(III) ions were also used for synthesis. Thus, the presence of elemental silver reserved on the surface of preformed Au NPs is essential for formation of ultrathin alloy-shells.

Fig. S4 Energy dispersive spectrometer (EDS) mapping images of HOH-shaped Au@AuPd NPs (A), ETHH-shaped Au@AuPd NPs (B) and OCT-shaped Au@AuPd NPs (C).



The molar fractions of residual Ag in the corresponding HOH-, ETHH-, and OCT-shaped Au@Au_mPd_n NPs with optimal electrocatalytic performances (samples in Fig. 4) were 3.8%, 4.9% and 5.5%, respectively, which were lower than those in their corresponding Au NPs, even leaven the additional amount of Au and Pd out of account.

Fig. S5 TEM images of HOH-shaped Au@Au_mPd_n NPs obtained by silver-assisted co-reduction of Au(III) ions of fixed amount and Pd(II) ions of varying amount onto the corresponding Au cores. The volume of Na₂PdCl₄ (1 mM) used for synthesis of HOH-shaped Au@AuPd NPs with different surface composition were changed from 10 μL (a) to 20 μL (b), 30 μL (c), 40 μL (d), and 50 μL (e).

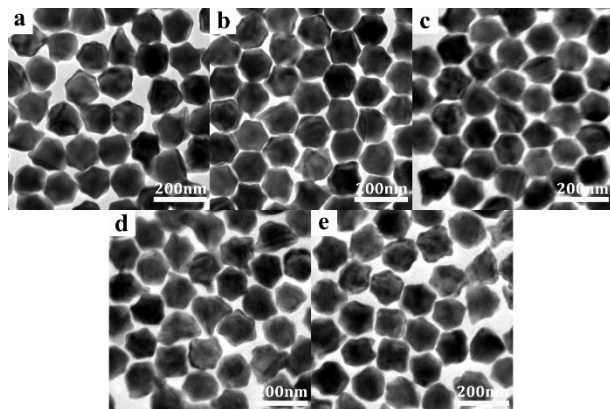


Fig. S6 TEM images of ETHH-shaped Au@Au_mPd_n NPs obtained by silver-assisted co-reduction of Au(III) ions of fixed amount and Pd(II) ions of varying amount onto the corresponding Au cores. The volume of Na₂PdCl₄ (1 mM) used for synthesis of ETHH-shaped Au@AuPd NPs with different surface composition was changed from 10 μL (a) to 20 μL (b), 30 μL (c), 40 μL (d), and 50 μL (e).

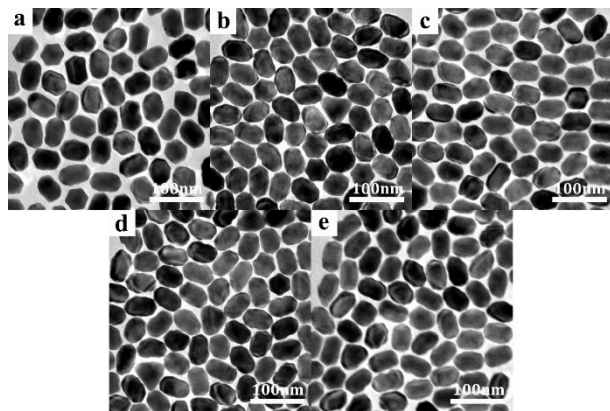


Fig. S7 TEM images of OCT-shaped $\text{Au}@\text{Au}_m\text{Pd}_n$ NPs obtained by silver-assisted co-reduction of Au(III) ions of fixed amount and Pd(II) ions of varying amount onto the corresponding Au cores. The volume of Na_2PdCl_4 (1 mM) used for synthesis of OCT-shaped $\text{Au}@\text{AuPd}$ NPs with different surface composition was changed from 10 μL (a) to 20 μL (b), 30 μL (c), 40 μL (d), and 50 μL (e).

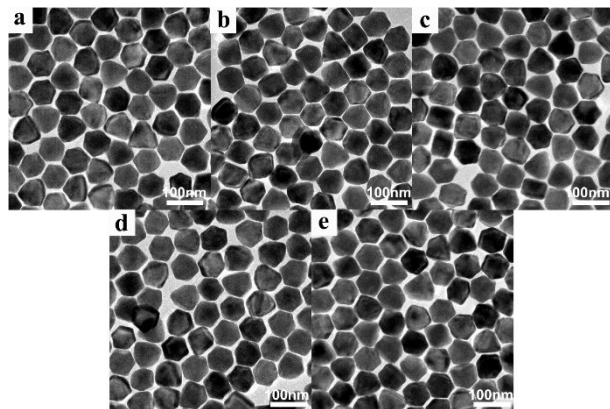


Fig. S8 CV curves (A to C) of GCEs modified by HOH-shaped Au@Au_mPd_n NPs measured in 0.50 M N₂-saturated KOH aqueous solution in the absence (A) and presence of 0.50 M ethanol (B and C) at room temperature. The currents of (A and B) and (C) were normalized by the Pd mass loaded on GCE and the ECSA values, respectively. The scan rates of (A) and (B and C) are 50 mV s⁻¹ and 20 mV s⁻¹, respectively. The resulting HOH-shaped Au@Au_mPd_n NPs with different surface composition were obtained by silver-assisted co-reduction of Au(III) ions of fixed amount and Pd(II) ions of varying amount onto the corresponding preformed Au cores. The volume of Na₂PdCl₄ (1 mM) used for synthesis of HOH-shaped Au@Au_mPd_n NPs with different surface composition was changed from 10 μL (a, black curve) to 20 μL (b, red curve), 30 μL (c, blue curve), 40 μL (d, cyan curve), and 50 μL (e, magenta curve).

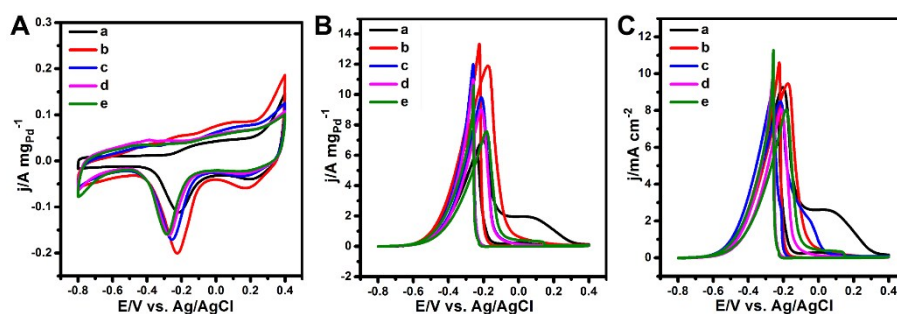


Fig. S9 CV curves (A to C) of GCEs modified by ETHH-shaped Au@Au_mPd_n NPs measured in 0.50 M N₂-saturated KOH aqueous solution in the absence (A) and presence of 0.50 M ethanol (B and C) at room temperature. The currents were normalized by the Pd mass loaded on GCE and the ECSA values, respectively. The scan rates of (A) and (B and C) are 50 mV s⁻¹ and 20 mV s⁻¹, respectively. The resulting ETHH-shaped Au@Au_mPd_n NPs with different surface composition were obtained by silver-assisted co-reduction of Au(III) ions of fixed amount and Pd(II) ions of varying amount onto the corresponding preformed Au cores. The volume of Na₂PdCl₄ (1 mM) used for synthesis of ETHH-shaped Au@Au_mPd_n NPs with different surface composition was changed from 10 μL (a, black curve) to 20 μL (b, red curve), 30 μL (c, blue curve), 40 μL (d, cyan curve), and 50 μL (e, magenta curve).

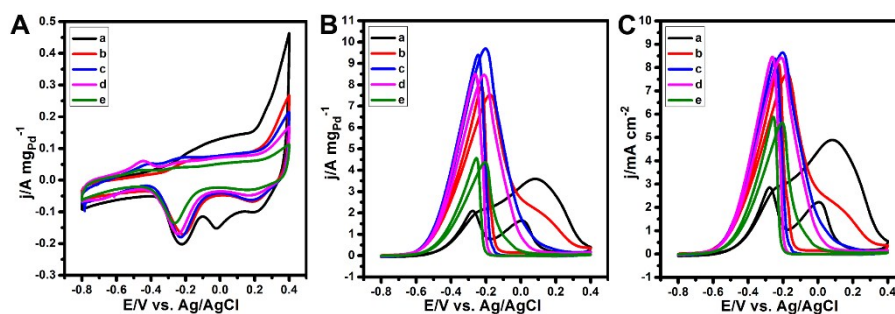


Fig. S10 CV curves (A to C) of GCEs modified by OCT-shaped Au@Au_mPd_n NPs measured in 0.50 M N₂-saturated KOH aqueous solution in the absence (A) and presence of 0.50 M ethanol (B and C) at room temperature. The currents of (A and B) and (C) were normalized by the Pd mass loaded on GCE and the ECSA values, respectively. The scan rates of (A) and (B and C) are 50 mV s⁻¹ and 20 mV s⁻¹, respectively. The resulting OCT-shaped Au@Au_mPd_n NPs with different surface composition were obtained by silver-assisted co-reduction of Au(III) ions of fixed amount and Pd(II) ions of varying amount onto the corresponding preformed Au cores. The volume of Na₂PdCl₄ (1 mM) used for synthesis of OCT-shaped Au@Au_mPd_n NPs with different surface composition was changed from 10 μL (a, black curve) to 20 μL (b, red curve), 30 μL (c, blue curve), 40 μL (d, cyan curve), and 50 μL (e, magenta curve).

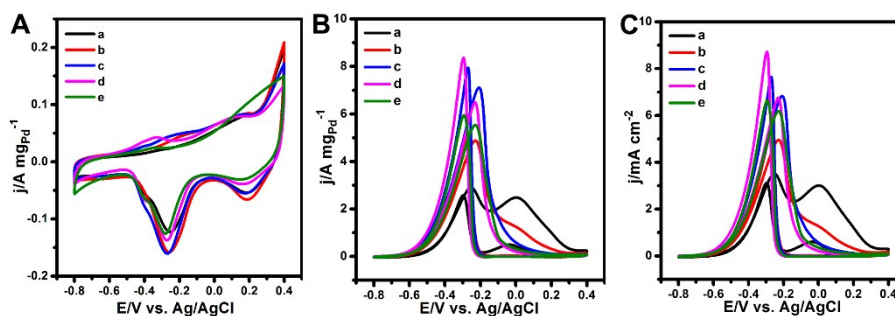


Fig. S11 Extinction spectra of HOH-shaped Au NPs (black curve) and HOH-shaped Au@Au_mPd_n NPs (red curve). The insets are digital pictures of their aqueous solutions of HOH-shaped Au NPs and HOH-shaped Au@Au_mPd_n NPs, respectively.

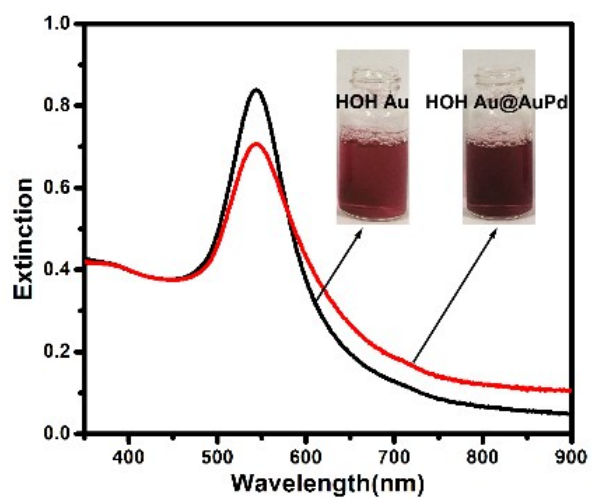


Fig. S12 Extinction spectra of ETHH-shaped Au NPs (black curve) and ETHH-shaped Au@Au_mPd_n NPs (red curve). The insets are digital pictures of their aqueous solutions of ETHH-shaped Au NPs and ETHH-shaped Au@Au_mPd_n NPs, respectively.

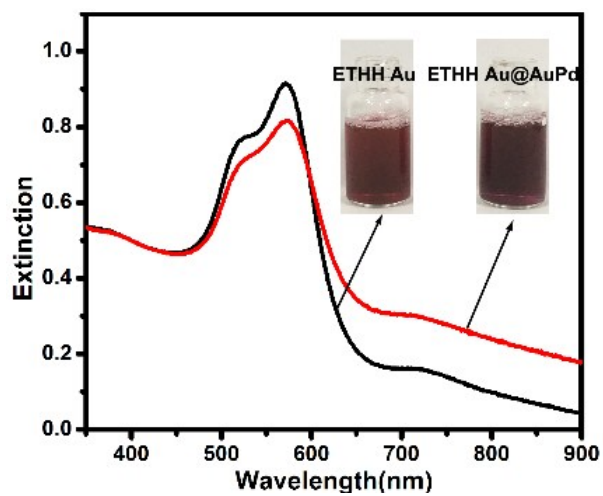


Fig. S13 Extinction spectra of OCT-shaped Au NPs (black curve) and OCT-shaped Au@Au_mPd_n NPs (red curve). The insets are digital pictures of their aqueous solutions of OCT-shaped Au NPs and OCT-shaped Au@Au_mPd_n NPs, respectively.

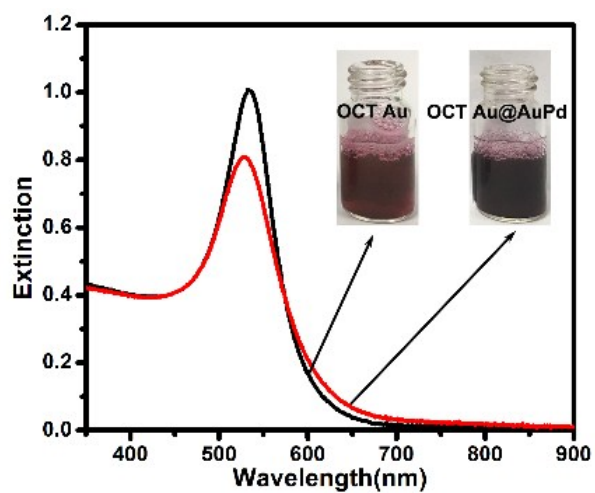
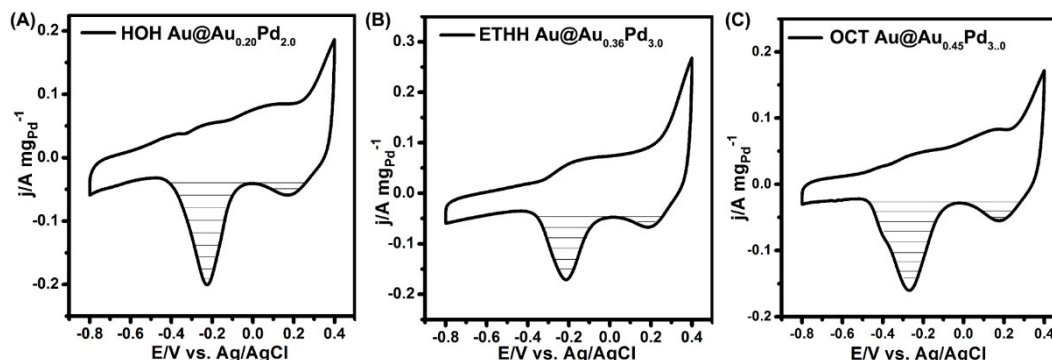


Fig. S14 (A to C) CV curves of the GCEs modified by HOH-, ETHH- and OCT-shaped Au@Au_mPd_n NPs measured in 0.50 M N₂-saturated KOH aqueous solution at room temperature, respectively. The regions denoted by the horizontal segments were used to calculate the surface areas of Pd and Au, using the surface charge associated with the reduction of their oxide.



The surface area of the catalysts can be determined by using the surface charge associated with the reduction of their oxide in the CV curves in an alkaline medium. The surface compositions of HOH-, ETHH-, and OCT-shaped Au@Au_mPd_n NPs can be calculated on the basis of the surface areas of Au and Pd obtained,^{1,2} which can be deduced as follows:

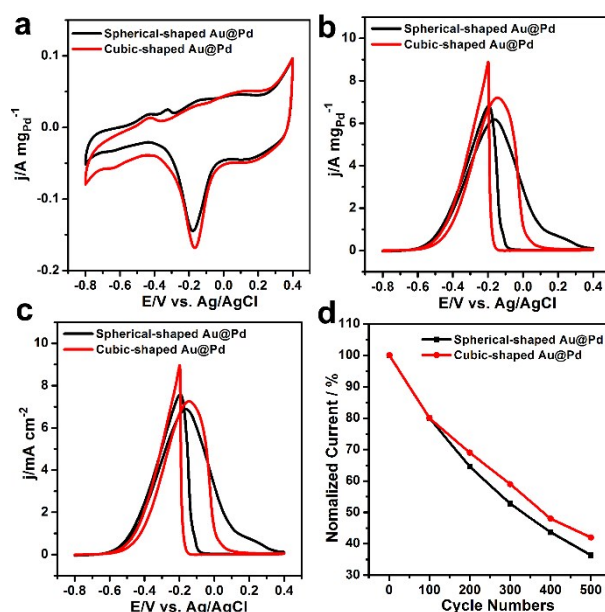
$$m = \frac{S_{Au}}{S_{Pd} + S_{Au}} \times 100$$

where m represents the Au percentage, and S_{Au} and S_{Pd} are the surface areas covered by Au and Pd oxides, respectively.

When a high upper potential limit is applied, the Au reduction peaks at about 0.2 V become stronger as the transfer of Au from the NP cores to the interfaces will occur. Thus, it has to carefully select the upper potential limit before testing. It is reported that the applied potential range for the formation of gold oxide monolayer of nanostructured

Au NPs is between 0.25 V and 0.4 V, which was demonstrated by the inhibition of methanol oxidation due to the formation of gold oxide monolayer.³

Fig. S15 CV curves (A to C) and potential cycling stability (D) of GCEs modified by spherical-shaped Au@Pd NPs and cubic-shaped Au@Pd NPs in 0.50 M N₂-saturated KOH aqueous solution in the absence (A) and in the presence (B to D) of 0.50 M ethanol at room temperature. The currents shown in (A and B) are normalized by the Pd mass loaded and (C) are normalized by the ECSA values, respectively. (D) Plot of the calibrated CV oxidation peak current density vs. the cycling number. The scan rates of (A and D) and (B and C) are 50 mV s⁻¹ and 20 mV s⁻¹, respectively.



The electrochemical activities of as-prepared spherical-shaped Au@Pd NPs and cubic-shaped Au@Pd NPs toward ethanol oxidation were also studied (Fig. S15). The ECSAs, current densities normalized by the Pd mass loaded, and current densities normalized by ECSA values of GCEs modified by spherical-shaped Au@Pd NPs and cubic-shaped Au@Pd NPs toward ethanol oxidation were summarized and listed in Table S6. The ECSA values (Fig. S15a and Table S6) of spherical-shaped Au@Pd NPs and cubic-shaped Au@Pd NPs are 92.4 and 101.2 m² g⁻¹, respectively; their mass activities are 6.2, and 7.3 A mg_{Pd}⁻¹, respectively (Fig. S15b and Table S6); and their specific activities are 6.7 and 7.2 mA cm⁻², respectively (Fig. S15c and Table S6).

The stability of spherical-shaped Au@Pd NPs and cubic-shaped Au@Pd NPs for ethanol electrooxidation were also investigated by CV cycling test (Fig. S15d and Table S6). It can be seen that the current densities of GCEs modified by spherical-shaped Au@Pd NPs and cubic-shaped Au@Pd NPs are reduced to about 36.5% and 40.7%, respectively, after 500 cycling tests.

Fig. S16 CV curves (A to C) and CA curves (D) of the GCEs modified by commercial Pd/C (a, black curve), HOH-shaped Au@Au_{0.20}Pd_{2.0} NPs (b, red curve), ETHH-shaped Au@Au_{0.36}Pd_{3.0} NPs (c, blue curve), and OCT-shaped Au@Au_{0.45}Pd_{3.0} NPs (d, dark cyan curve), respectively, which were measured in 0.10 M HClO₄ in the absence (A) and the presence of 0.10 M formic acid (B to D). The currents were normalized by the Pd mass loaded on the GCE (A, B and D) and ECSA values (C), respectively. The scan rates A and (B and C) were 50 mV s⁻¹ and 20 mV s⁻¹, respectively. CA curves (D) were recorded at 0.4 V.

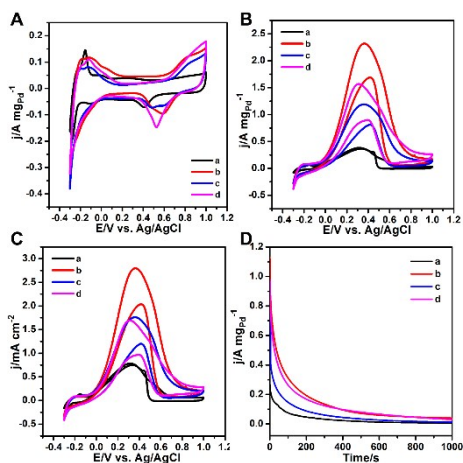


Fig. S17 TEM images of HOH-shaped Au@Au_{0.20}Pd_{2.0} NPs (a), ETHH-shaped Au@Au_{0.36}Pd_{3.0} NPs (b), and OCT-shaped Au@Au_{0.45}Pd_{3.0} NPs (c) after durability test.

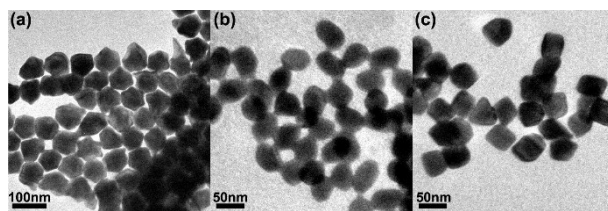


Table S1 Summary of atomic molar ratios (at%) of HOH-, ETHH-, and OCT-shaped Au NPs obtained by EDS and ICP-AES.

Sample	Au (at%)	Ag (at%)
HOH-shaped Au NPs	95.5	4.5
ETHH-shaped Au NPs	94.0	6.0
OCT-shaped Au NPs	91.6	8.4

Table S2 Geometric model, relations between the projection angles and Miller indices, and calculated projection angles of HOH-shaped Au NPs with different Miller indices. The measured projection angles formed between edge-on facets agree well with the calculated values for the {651} facets.

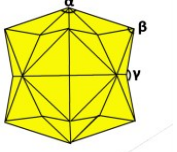
Geometric model		Calculated projection angles			
		Miller index {hkl}	α	β	γ
Relations between the projection angles and Miller indices	$\alpha = 2 \arctan\left(\frac{\sqrt{2}h}{k-l}\right)$ $\beta = 90 - \left(\frac{\alpha}{2}\right) + \left(\frac{\gamma}{2}\right)$ $\gamma = 2 \arctan\left(\frac{h+k}{\sqrt{2}l}\right)$	{321}	153.5	87.5	148.4
		{421}	160.0	86.8	153.5
		{431}	141.1	98.1	157.2
		{541}	134.0	104.1	162.1
		{542}	148.4	88.4	145.1
		{651}	129.5	107.9	165.4

Table S3 Summary of ECSAs, mass- and ECSA-normalized current densities of GCEs modified by HOH-shaped Au@Au_mPd_n NPs obtained for different volumes of Na₂PdCl₄ solution (1 mM): 10 μ L (a), 20 μ L (b), 30 μ L (c), 40 μ L (d), and 50 μ L (e) as catalysts on ethanol oxidation in 0.50 M KOH solution containing 0.50 M ethanol, respectively.

Sample	ECSA [m² g⁻¹]	Mass activity [A mg_{Pd}⁻¹]	Specific activity [mA cm⁻²]
a	76.6	7.0	9.1
b	125.8	11.9	9.5
c	112.1	9.5	8.5
d	100.5	8.1	8.1
e	94.3	7.6	8.0

Table S4 Summary of ECSAs, mass- and ECSA-normalized current densities of GCEs modified by ETHH-shaped Au@Au_mPd_n NPs obtained for different volumes of Na₂PdCl₄ solution (1 mM): 10 μL (a), 20 μL (b), 30 μL (c), 40 μL (d), and 50 μL (e) as catalysts on ethanol oxidation in 0.50 M KOH solution containing 0.50 M ethanol, respectively.

Sample	ECSA [m² g⁻¹]	Mass activity [A mg_{Pd}⁻¹]	Specific activity [mA cm⁻²]
a	73.4	3.6	4.9
b	97.3	7.5	7.7
c	107.2	9.7	9.0
d	100.5	8.5	8.4
e	77.6	4.4	5.7

Table S5 Summary of ECSAs, mass- and ECSA-normalized current densities of GCEs modified by OCT-shaped Au@Au_mPd_n NPs obtained for different volumes of Na₂PdCl₄ solution (1 mM): 10 μ L (a), 20 μ L (b), 30 μ L (c), 40 μ L (d), and 50 μ L (e) as catalysts for ethanol oxidation in 0.50 M KOH solution containing 0.50 M ethanol, respectively.

Sample	ECSA [m² g⁻¹]	Mass activity [A mg_{Pd}⁻¹]	Specific activity [mA cm⁻²]
a	82.6	2.9	3.5
b	98.5	4.9	5.0
c	105.1	7.1	6.8
d	95.3	6.4	6.7
e	89.5	5.5	6.1

Table S6. Summarized data of the ECSAs, current densities normalized by Pd mass (mass activity) and current densities normalized by their ECSA values (specific activity) of the GCEs modified by HOH-shaped Au@Au_{0.20}Pd_{2.0} NPs, ETHH-shaped Au@Au_{0.36}Pd_{3.0} NPs, OCT-shaped Au@Au_{0.45}Pd_{3.0} NPs, spherical-shaped Au@Pd NPs and cubic-shaped Au@Pd NPs with respect to ethanol oxidation in 0.50 M KOH solution containing 0.50 M ethanol.

Sample	ECSA [m ² g ⁻¹]	Mass activity [A mg ⁻¹]	Specific activity [mA cm ⁻²]	500 cycles
HOH-shaped Au@Au _{0.20} Pd _{2.0} NPs	125.8	11.9	9.5	51.0%
ETHH-shaped Au@Au _{0.36} Pd _{3.0} NPs	107.2	9.7	9.0	40.8%
OCT-shaped Au@Au _{0.45} Pd _{3.0} NPs	105.1	7.1	6.8	59.2%
spherical-shaped Au@Pd NPs	92.4	6.2	6.7	36.5%
cubic-shaped Au@Pd NPs	101.2	7.3	7.2	40.7%

Table S7 Summary of ECSAs, mass- and ECSA-normalized current densities of GCEs modified by HOH-shaped Au@Au_{0.20}Pd_{2.0} NPs, ETHH-shaped Au@Au_{0.36}Pd_{3.0} NPs, OCT-shaped Au@Au_{0.45}Pd_{3.0} NPs, and commercial Pd/C catalysts on oxidation of formic acid in 0.10 M HClO₄ solution containing 0.10 M formic acid.

Sample	ECSA [m² g⁻¹]	Mass activity [A mg_{Pd}⁻¹]	Specific activity [mA cm⁻²]
Pd/C	48.57	0.38	0.78
HOH-shaped Au@Au _{0.20} Pd _{2.0}	82.9	2.32	2.80
ETHH-shaped Au@Au _{0.36} Pd _{3.0}	67.6	1.20	1.78
OCT-shaped Au@Au _{0.45} Pd _{3.0}	92.7	1.56	1.68

References

- 1 A. Habrioux, W. Vogel, M. Guinel, L. Guetaz, K. Servat, B. Kokoh and N. Alonso-Vante, *Phys. Chem. Chem. Phys.*, 2009, **11**, 3573–3579.
- 2 C. X. Bi, C. Feng, T. T. Miao, Y. H. Song, D. Y. Wang and H. B. Xia, *Nanoscale*, 2015, **7**, 20105–20116.
- 3 J. T. Zhang, P. P. Liu, H. Y. Ma and Y. Ding, *J. Phys. Chem. C*, 2007, **111**, 10382-10388.